AUT Journal of Civil Engineering

AUT J. Civil Eng., 8(1) (2024) 17-32
DOI: 10.22060/ajce.2024.22777.5847

Computational efficiency of mixed least squares meshless models over SPH method for elliptic PDEs

Gholamreza Shobeyri*, Seyed Hossein Ghoreishi Najafabadi, Mehrdad Abed

Faculty of Civil, Water & Environmental Engineering, Shahid Beheshti University, Tehran, Iran

ABSTRACT: Analysis of various physical phenomena requires a solution of partial differential equations. Numerical methods especially the meshless schemes are used to discretize and solve these equations. Recently, several modifications have been proposed and applied to improve the numerical performance of the smoothed particle hydrodynamics (SPH) as a well-known meshless method. This study aims to show that the least squares methods especially in the context of the mixed formulation can get more accuracy compared with all existing SPH models. To validate this claim, three meshless numerical models are derived from Taylor series expansion on the basis of the mixed formulation. One of the models is based on first-order ordinary mixed formulation while two others use the first and second-order least squares mixed scheme. For accuracy analysis of the proposed methods, a potential flow and three 2D differential equations have been solved and examined with the presented SPH models. The main finding of this study is that the proposed mixed second-order least squares method has the ability to achieve significant computational efficiency over several SPH models. In addition, it has been found that the least square scheme can improve the accuracy of the ordinary mixed model.

Review History:

Received: Nov. 28, 2023
Revised: Feb. 08, 2024
Accepted: Nov. 03, 2024
Available Online: Nov. 03, 2024

Keywords:

Meshless Numerical Methods
Smoothed Particle Hydrodynamics
Elliptic Differential Equations
Potential Flows
Mixed Formulation

1- Introduction

Many natural phenomena can be described in the form of differential equations. For analysis of these phenomena, the empirical or laboratory methods are employed which have their specific advantages and disadvantages. The analytical methods have been presented to solve the partial differential equations. However, they cannot provide a comprehensive solution for all partial differential equations. Hence, by development of high-speed computers, numerical methods which are a subset of mathematical methods were developed for solution of these differential equations. The numerical methods in turn are divided into the mesh-based and meshless methods. While the mesh-based numerical methods have been widely used but they have limitations in the solution of free surface flows where the boundary conditions are changing consistently. The advantage of using meshless methods is that they solve differential equations without need for the meshing process which results in reduced computational costs. One of the meshless numerical methods is the SPH method which is among the pioneering methods in this respect.

The SPH method was first presented by Lucy and Monaghan for the solution of astrophysics problems [1]. In 1994, Monaghan used this method for analysis of the free surface flows and stated that it could also be generalized for the solution of incompressible fluids [2]. In the SPH method, the computational domain is discretized into a number of nodes, and the unknown values at each node are calculated based on the theory of the interpolation of integration. The SPH method is employed in two forms: the compressible method and the incompressible method. In the compressible method, the fluid is assumed to be compressible to some extent and the pressure field is obtained using an equation of state. But in the incompressible method, the fluid is assumed to be fully incompressible and the pressure field is obtained by solution of a second-order differential equation, where each of the above-mentioned methods has its own specific advantages and disadvantages. Considering the efficiency of the SPH method, many problems in the field of hydraulic engineering have been solved or investigated including the investigation of Newtonian and non-Newtonian free surface flows [3], turbulent open channel flow over the natural gravel bed with rough boundaries [4], oscillatory behavior of a flapper wave energy converter [5], the drop/wall interaction [6], fluid flow interactions with saturated/unsaturated porous media [7], multiphase melting flows [8], hydrodynamics of floating offshore wind turbines [9] and two-dimensional water–sediment two-phase flows [10]. Despite the capability and long history of implementing the classic SPH method, there are still a number of shortcomings in this method such as tensile instability. These shortcomings are especially more evident when dealing with the second-order spatial derivatives.

*Corresponding author's email: g_shobeyri@sbu.ac.ir

In the incompressible SPH method, the combination of the flow equations results in the Laplace equation of pressure and its solution yields the pressure value and ultimately the velocity field is obtained. The derivatives of SPH method have not a high precision and may yield unrealistic pressure fluctuations; hence many researchers have proposed modifications based on the mathematical formulations to resolve these shortcomings [11]. Among others, Hu and Adams proposed a higher-order Laplacian model of incompressible SPH method using the average temporal derivative of particles [12]. Schwaiger introduced another higher-order Laplacian model of the incompressible SPH method where the approximation of the gradient of higher-order terms is included using the Taylor series expansion [13]. The higher order Laplacian model of incompressible SPH method proposed by Hosseini and Feng is based on the precise estimation of linear function gradient [14], Shobeyri introduced a new Laplacian model using the combination of incompressible SPH method with Taylor series expansion and the moving least squares (MLS) method [15]. Shobeyri also presented an enhanced Laplacian model using the Voronoi diagram [16].

In this article, three new numerical models are formulated using the mixed formulation in which the second-order derivative is converted into the first-order derivative. One of the models is obtained on the basis of a mixed first-order ordinary scheme while two others apply mixed first and second-order least squares formulations. The higher computational efficiency of these models especially the second-order least squares method is validated for several quadratic differential equations over the original SPH method and a recently developed higher-order SPH Laplacian model [17]. This improved SPH model has shown significant accuracy compared even with the well-known existing SPH methods [17]. The superiority of the second-order least squares method in comparison with the improved SPH scheme indicates the efficiency of the least squares scheme especially in the form of mixed formulation over several existing meshless methods. First, the fundamental formulations of the standard and the improved SPH models are given and then, the mixed models are introduced in this paper. Finally, the numerical performance of the presented models is examined for the solution of different second-order PDEs.

2- Smoothed particle hydrodynamics (SPH) methods

2- 1- Standard SPH method (Model 1)

Any given function $f(r)$ could be expressed utilizing the SPH method and using the integral equation as follows:

$$f(r_a)=\int_\Omega f(r)W(r,\,R_s).dr \tag{1}$$

In the above equation, r is the distance between the reference node a and the neighboring nodes in its surrounding area with radius of R_s and W is the kernel function. The following equation is one of the common 2D kernel functions [18]:

$$W(r,R_s)=\frac{8}{\pi R_s^2}\left(\frac{3}{4}\left(\frac{r}{R_s}\right)^2-\frac{3}{2}\left(\frac{r}{R_s}\right)+\frac{3}{4}\right) \tag{2}$$

The integral form of Eq. (1) cannot be used in the numerical method; accordingly, it was discretized as follows:

$$f(r_a)=\sum_b f(r_b)W_{ab}\Delta V_b \tag{3}$$

Where b denotes the surrounding calculation nodes, W_{ab} gives the value of kernel function at node b with respect to the position of a target node (a) and ΔV represents the volume of particles.

For computing the volume assigned to each node, Eq. (3) is applied as follows:

$$\frac{1}{\Delta V_a}=\sum_b\frac{1}{\Delta V_b}W_{ab}\Delta V_b=\sum_b W_{ab}\;\rightarrow\;\Delta V_a=\frac{1}{\sum_b W_{ab}} \tag{4}$$

As a result, the spatial derivative of the function $f(r)$ could be approximated as shown below:

$$\nabla f(r_a)=\sum_b f(r_b)\nabla W_{ab}\Delta V_b \tag{5}$$

Where ∇W_{ab} represents the gradient of kernel function with respect to node a.

The most utilized Laplacian model in the incompressible SPH approach is obtained by combining the standard SPH method and the finite difference method for approximating the first-order derivatives which have a lower sensitivity with respect to the irregularity of nodal distribution is as follows [3]:

$$\nabla^2 f_a=\sum_b\frac{2\Delta V_b r_{ab}.\nabla W_{ab}}{|r_{ab}|^2}(f_a-f_b) \tag{6}$$

2- 2- Improved SPH Model (Model 2)

The moving particle semi-implicit (MPS) method is a powerful and well-known meshless method and has been extensively applied for the investigation of a wide range of engineering applications. Recently, a kernel gradient-free SPH Laplacian model with high accuracy has been suggested by considering the similarity between SPH and MPS methods as follows [17]:

$$\nabla^2 f_a = \sum_b \frac{-2\mathbf{r}_{ab}.(\text{Cof\_Grad\_MPS})(f_b - f_a)}{|\mathbf{r}_{ab}|^2} \tag{7}$$

Where Cof_Grad_MPS is expressed by the following equation:

$$\begin{aligned}\text{Cof\_Grad\_MPS} = [&\frac{1}{\lambda}\sum_{b\neq a}\frac{1}{n_b}W_{ab}(\mathbf{r}_b - \mathbf{r}_a) \\ &\otimes(\mathbf{r}_b - \mathbf{r}_a)^T]^{-1}[\frac{1}{\lambda}\sum_{b\neq a}\frac{1}{n_b}W_{ab}(\mathbf{r}_b - \mathbf{r}_a)]\end{aligned} \tag{8}$$

In the above equation, n and λ are two computational parameters of MPS method and defined as follows:

$$n_a = \sum_{b\neq a} W_{ab} \tag{9}$$

$$\lambda = \frac{\int_\Omega W(r) r^2 d\Omega}{\int_\Omega W(r) d\Omega} \tag{10}$$

2- 3- Mixed formulation

The so-called mixed formulation is an efficient technique for reducing computational costs while increasing the precision of the approximation of second-order derivatives. Indeed, the fact that only first-order derivatives of the functions are used in the computations increases the numerical precision. A second-order differential equation in 2D form can be expressed as follows:

$$a_x \frac{\partial^2 f}{\partial x^2} + b_y \frac{\partial^2 f}{\partial y^2} + c_{xy} \frac{\partial^2 f}{\partial x \partial y} = g(x, y) \tag{11}$$

Where a_x , b_y and c_{xy} are the coefficients of the differential equation and $g(x, y)$ is the source term. The above equation can be converted to a first-order system of equations in the (Eqs. (12)-(14)) using a straightforward mathematical procedure. An even simpler approach would be to find the arrays of matrixes A^x , A^y , B and S coupled with Eqs. (12) - (14) to derive Eq. (11).

$$A^x \frac{\partial F}{\partial x} + A^y \frac{\partial F}{\partial y} + BF = S \tag{12}$$

Where F is the vector of unknowns and is defined as follows:

$$F = \left[f, f_x, f_y\right]^T \tag{13}$$

Also, in Eq. (12) we have:

$$\begin{aligned} S^T &= \left[0, 0, g(x, y)\right] \\ A^x &= \begin{bmatrix} 1 & 0 & 0 \\ 0 & 0 & 0 \\ 0 & a_x & c_{xy} \end{bmatrix} \\ A^y &= \begin{bmatrix} 0 & 0 & 0 \\ 1 & 0 & 0 \\ 0 & 0 & b_y \end{bmatrix} \\ B &= \begin{bmatrix} 0 & -1 & 0 \\ 0 & 0 & -1 \\ 0 & 0 & 0 \end{bmatrix} \end{aligned} \tag{14}$$

Where S^T is the transpose of S . The above formulation has been employed in the Discrete Least Squares Meshless (DLSM) method [19-25]. To solve the differential equation in the mixed model (Eq. (12)), one needs to approximate the function and its first derivatives. The following sections explain different approaches to this objective.

2- 3- 1- Mixed ordinary method (Model 3)

Before Eq. (12) can be solved, we need the first-order derivatives of the function *F*. As far as this purpose is concerned, the application of the standard SPH gradient model (Eq. (5)) is highly erroneous due to the formation of a diagonal matrix of coefficients with zero value. The accuracy of such a model is especially low for approximating the gradient near the boundaries where the node distribution is irregular. Various modifications have been proposed to address this problem. Among others, a combination of SPH interpolation with Taylor expansion is proposed for this purpose, as follows [26]:

$$\begin{aligned}\sum_b f(r_b)W \approx &\sum_b f(r_a)W \\ &+ \sum_b f_x(r_a)\Delta x_b W + \sum_b f_y(r_a)\Delta y_b W\end{aligned} \tag{15}$$

Where $W = W_{ab}$.

Multiplying both sides of Eq. (15) by $\Delta x_b = x_b - x_a$ and then $\Delta y_b = y_b - y_a$ gives Eqs. (16) and (17), respectively.

$$\begin{aligned}\sum_b f(r_b)\Delta x_b W \approx &\sum_b f(r_a)\Delta x_b W \\ &+ \sum_b f_x(r_a)\Delta x_b^2 W + \sum_b f_y(r_a)\Delta x_b \Delta y_b W\end{aligned} \tag{16}$$

$$\sum_b f\left(r_b\right)\Delta y_b W \approx \sum_b f\left(r_a\right)\Delta y_b W + \sum_b f_x\left(r_a\right)\Delta x_b \Delta y_b W + \sum_b f_y\left(r_a\right)\Delta y_b^2 W \quad (17)$$

Eqs. (15) – (17) could be rewritten in the form of a matrix:

$$\begin{bmatrix} f\left(r_a\right) \\ f_x\left(r_a\right) \\ f_y\left(r_a\right) \end{bmatrix} = \begin{bmatrix} \sum_b W & \sum_b \Delta x_b W & \sum_b \Delta y_b W \\ \sum_b \Delta x_b W & \sum_b \Delta x_b^2 W & \sum_b \Delta x_b \Delta y_b W \\ \sum_b \Delta y_b W & \sum_b \Delta x_b \Delta y_b W & \sum_b \Delta y_b^2 W \end{bmatrix}^{-1} \begin{bmatrix} \sum_b f\left(r_b\right) W \\ \sum_b f\left(r_b\right)\Delta x_b W \\ \sum_b f\left(r_b\right)\Delta y_b W \end{bmatrix} \quad (18)$$

Where f_x and f_y are the derivatives of function f with respect to x and y coordinate axes. It has been found this method has higher accuracy and lower calculation costs compared with MLS method which is a well-known approach for function approximation [27, 28].

This equation can also be applied to calculate the parameters F, $\frac{\partial F}{\partial x}$ and $\frac{\partial F}{\partial y}$ in Eq. (12) and ultimately the corresponding matrix of coefficients obtained in this way will be solved to determine F representing the values of f, f_x and f_y. Noteworthily, the above equations consider the reference node to prevent the formation of the diagonal matrix of coefficients with zero value. The main property of the mixed formulation is that the number of unknowns increases from one *(f)* in the standard state to three *(f, f_x and f_y),* results in an increase of the set of equations by three times. But as the approximation of the first-order derivatives has a lower error, then there is need for a lower number of computational nodes leading to a lower computational cost. Noting that in this method, in addition to the value of the function, the derivatives also are among the unknowns therefore both Dirichlet and Neumann boundary conditions can be directly satisfied by eliminating the known values at the boundaries from the corresponding coefficients matrix.

2- 3- 2- Mixed least squares models (Models 4 & 5)

As described in the previous section, the function and its derivatives must be evaluated in the mixed model. An efficient approach for function approximation is the use of the weighted least squares method. The Taylor series expansion by ignoring the higher order terms and around the central node (x_0, y_0) for a given function is in the following form:

$$f\left(x,y\right) = f_0 + \frac{\partial f_0}{\partial x}\Delta x + \frac{\partial f_0}{\partial y}\Delta y + \frac{\partial^2 f_0}{\partial x^2}\frac{\Delta x^2}{2} + \frac{\partial^2 f_0}{\partial x\,\partial y}\Delta x\,\Delta y + \frac{\partial^2 f_0}{\partial y^2}\frac{\Delta y^2}{2} \quad (19)$$

Where $\Delta x = x - x_0$ and $\Delta y = y - y_0$. By considering this equation for all the surrounding nodes, the following linear equations are obtained:

$$\begin{bmatrix} 1 & \Delta x_1 & \Delta y_1 & \frac{1}{2}\Delta x_1^2 & \Delta x_1\Delta y_1 & \frac{1}{2}\Delta y_1^2 \\ 1 & \Delta x_2 & \Delta y_2 & \frac{1}{2}\Delta x_2^2 & \Delta x_2\Delta y_2 & \frac{1}{2}\Delta y_2^2 \\ \dots & \dots & \dots & \dots & \dots & \dots \\ 1 & \Delta x_N & \Delta y_N & \frac{1}{2}\Delta x_N^2 & \Delta x_N\Delta y_N & \frac{1}{2}\Delta y_N^2 \end{bmatrix} \begin{bmatrix} f_0 \\ \partial f_0/\partial x \\ \partial f_0/\partial y \\ \partial^2 f_0/\partial x^2 \\ \partial^2 f_0/\partial x\partial y \\ \partial^2 f_0/\partial y^2 \end{bmatrix} = \begin{bmatrix} f_1 \\ f_2 \\ \dots \\ f_N \end{bmatrix} \quad (20)$$

Where N denotes the number of nodes around the influence area of the central node.

In order to increase the precision of the approximation, a large number of neighboring nodes are used in computations that are more in number than the number of unknowns in the above equation (6 unknowns) which results in an over-determined set of linear equations. To solve this equation the following error norm is used [29]:

$$\|E\| = \sum_{j=1}^{N} \left[f_0 - f_j + \frac{\partial f_0}{\partial x}\Delta x_j + \frac{\partial f_0}{\partial y}\Delta y_j + \frac{\partial^2 f_0}{\partial x^2}\frac{\Delta x_j^2}{2} + \frac{\partial^2 f_0}{\partial x\,\partial y}\Delta x_j \Delta y_j + \frac{\partial^2 f_0}{\partial y^2}\frac{\Delta y_j^2}{2} \right]^2 W_j^2 \quad (21)$$

Where W_j is the weight function.

The unknown parameters of Eq. (20) (based on the weighted least squares) are obtained by minimizing the above error norm.

$$\frac{\partial \|E\|}{\partial F\_leas\_squ} = 0 \quad (22)$$

Where $F\_leas\_squ = [f_0, \frac{\partial f_0}{\partial x}, \frac{\partial f_0}{\partial y}, \frac{\partial^2 f_0}{\partial x^2}, \frac{\partial^2 f_0}{\partial x\,\partial y}, \frac{\partial^2 f_0}{\partial y^2}]$ denotes the unknowns' vector. Solving the above equation, we would have:

$$F\_leas\_squ = M^{-1} \times RHS \quad (23)$$

Cooficents matrix *M and* vector *RHS* are defined in Eqs. (23) and (24), respectively.

$$M=\begin{bmatrix} \sum W_j^2 & \sum W_j^2\Delta x_j & \sum W_j^2\Delta y_j & \sum W_j^2\,\Delta x_j^2/2 & \sum W_j^2\Delta x_j\Delta y_j & \sum W_j^2\,\Delta y_j^2/2 \\ \sum W_j^2\Delta x_j & \sum W_j^2\Delta x_j^2 & \sum W_j^2\Delta x_j\Delta y_j & \sum W_j^2\Delta x_j^3/2 & \sum W_j^2\Delta x_j^2\Delta y_j & \sum W_j^2\Delta x_j\,\Delta y_j^2/2 \\ \sum W_j^2\Delta y_j & \sum W_j^2\Delta x_j\Delta y_j & \sum W_j^2\Delta y_j^2 & \sum W_j^2\,\Delta x_j^2\Delta y_j/2 & \sum W_j^2\Delta x_j\Delta y_j^2 & \sum W_j^2\Delta y_j^3/2 \\ \sum W_j^2\,\Delta x_j^2/2 & \sum W_j^2\Delta x_j^3/2 & \sum W_j^2\,\Delta x_j^2\Delta y_j/2 & \sum W_j^2\,\Delta x_j^4/4 & \sum W_j^2\Delta x_j^3\,\Delta y_j/2 & \sum W_j^2\Delta x_j^2\,\Delta y_j^2/4 \\ \sum W_j^2\Delta x_j\Delta y_j & \sum W_j^2\Delta x_j^2\Delta y_j & \sum W_j^2\Delta x_j\Delta y_j^2 & \sum W_j^2\Delta x_j^3\,\Delta y_j/2 & \sum W_j^2\Delta x_j^2\Delta y_j^2 & \sum W_j^2\,\Delta x_j\Delta y_j^3/2 \\ \sum W_j^2\,\Delta y_j^2/2 & \sum W_j^2\Delta x_j\,\Delta y_j^2/2 & \sum W_j^2\Delta y_j^3/2 & \sum W_j^2\Delta x_j^2\,\Delta y_j^2/4 & \sum W_j^2\,\Delta x_j\Delta y_j^3/2 & \sum W_j^2\,\Delta y_j^4/2 \end{bmatrix} \tag{24}$$

$$RHS=\left[\sum f_jW_j^2 \quad \sum f_jW_j^2\Delta x_j \quad \sum f_jW_j^2\Delta y_j \quad \sum f_jW_j^2\,\Delta x_j^2/2 \quad \sum f_jW_j^2\Delta x_j\Delta y_j \quad \sum f_jW_j^2\,\Delta y_j^2/2\right]^T \tag{25}$$

Using the first 3 terms in Eq. (19), the coefficient matrix in Eq. (23) would be of size 3 by 3 and the considered unknown values ($f_0, \frac{\partial f_0}{\partial x}, \frac{\partial f_0}{\partial y}$), required in the discretization of Eq. (12) using the method explained in the previous section, would be computed with lower accuracy. This approach is called the mixed first-order least squares method (Model 4). Should one use the first 6 terms in Eq. (19), a 6-by-6 coefficient matrix appears in Eq. (24) and higher accuracy can be achieved in the calculation of the function and its first derivatives. This scheme is called the mixed second-order least squares method (Model 5).

3- Numerical examples

For validation and comparison of the precision of the introduced models, a number of examples are solved in this section. The considered examples are a potential flow and three different 2D elliptic differential equations with analytical solutions. These problems with second-order partial differential equations are chosen to examine the numerical performance of the methods for the Laplace operator which is applied to describe many different physical applications in fluid and solid machines. The numerical error for each method in the considered problems is calculated using the following formula [30]:

$$E_r=\sum_{i=1}^{n}\frac{f_i-f_{ana}}{f_{ana}}\times\frac{100}{n} \tag{26}$$

Where E_r denotes the mean error in percentage, f_i denotes the numerical solution for node i, f_{ana} is the corresponding analytical solution and n represents the number of computational nodes.

3- 1- Potential flow problem

The potential flow is an incompressible flow where viscosity has an insignificant effect. The equations governing the potential flow are 2D elliptic differential equations. Among the applications of potential flow, one could refer to flow over weirs in dams, groundwater flow, transfer and emission of pollution and heat, and also air flow over the airplane wing. The stream function in this type of problem is as follows:

$$\frac{\partial^2\psi}{\partial x^2}+\frac{\partial^2\psi}{\partial y^2}=0 \tag{27}$$

By differentiating the stream function (ψ), the horizontal and vertical velocities are obtained.

$$\frac{\partial\psi}{\partial y}=u \quad \frac{\partial\psi}{\partial x}=-v \tag{28}$$

In this section, the following potential flow problem is dealt with where their computational domains. The problem is the combination of a vortex and dipole at the center together with a uniform flow. A dipole by itself is the result of the superposition of a sink and a source with an equal force. The analytical solution for the stream function in this problem is as follows:

$$\psi=\frac{\Gamma}{2\pi}\ln\sqrt{\left(x-x_c\right)^2+\left(y-y_c\right)^2}+\frac{\kappa}{2\pi}\left(\frac{y-y_c}{\left(x-x_c\right)^2+\left(y-y_c\right)^2}\right)+Vy \tag{29}$$

Where (x_c, y_c) is the coordinates of the vortex center, Γ is the vortex intensity, V is the uniform flow intensity, and κ is the dipole intensity.

The problem is solved on a 2.5 m by 2.5 m square computational domain. A circle with a radius of 0.6 m is excluded from the domain to avoid large values of the analytical solution at the center of the circle which coincides with the

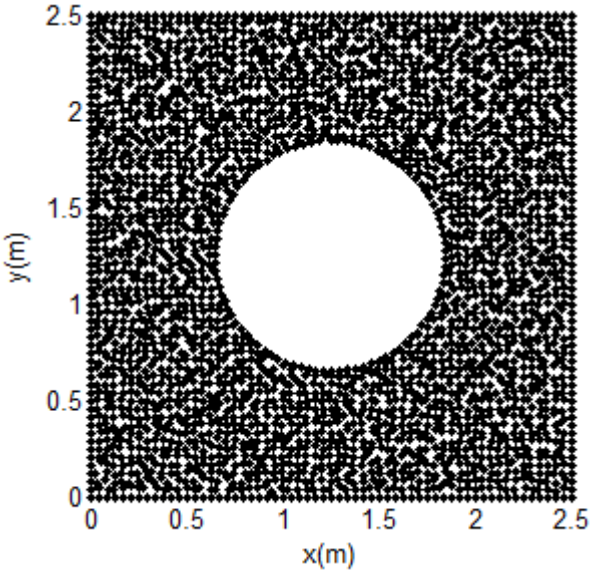

Fig. 1. Random node configuration with $L_0 = 1/24$ m for the solution of the potential flow.

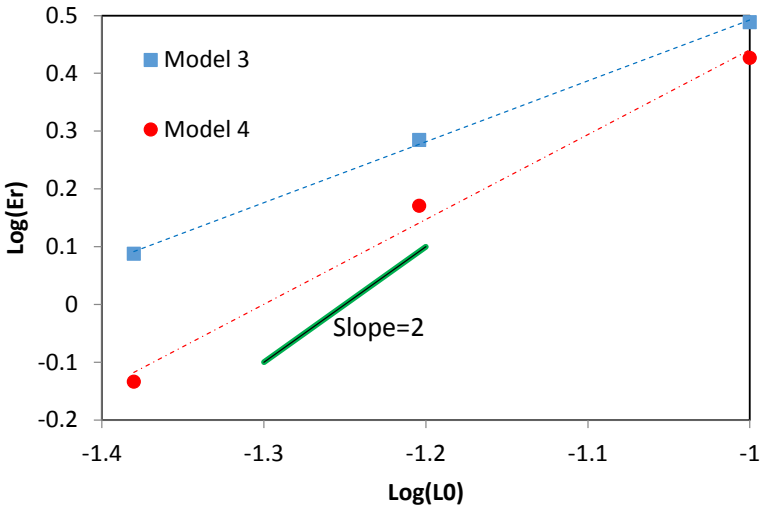

Fig. 2. Error analysis for the potential flow test problem.

center of the square domain. Irregular node distributions for domain discretization are obtained by moving the calculation nodes initially at a uniform configuration based on a random number generator with a maximum distance of KL_0 where L_0 is the initial distance between the computational nodes and K is the irregularity index and chosen 0.3 in this study. Three runs with L_0 of 1/10 m, 1/16 m, and 1/24 m are carried out to examine the accuracy analysis of the models. A sample node configuration corresponding to $L_0 = 1/24$ m is shown in Figure 1. This section aims to compare the performance of the mixed ordinary model (Model 3) and mixed first-order least squares method (Model 4). As seen in Figure 2, Model 4 can attain smaller errors for this test problem exhibiting the effectiveness of the least squares scheme to improve numerical accuracy in the context of mixed formulation. In the remaining of this article, the results of Model 3 due to its lower accuracy compared with Model 4 are not included. Figure 3 plots the solution of Eq. (27) by Model 4 for the fine node distribution ($L_0 = 1/24$ m) with the minimum error obtained from $R_s / L_0 = 1.7$. The corresponding calculated velocity field is also illustrated in Figure 4 using the solution derivatives in Eq. (28).

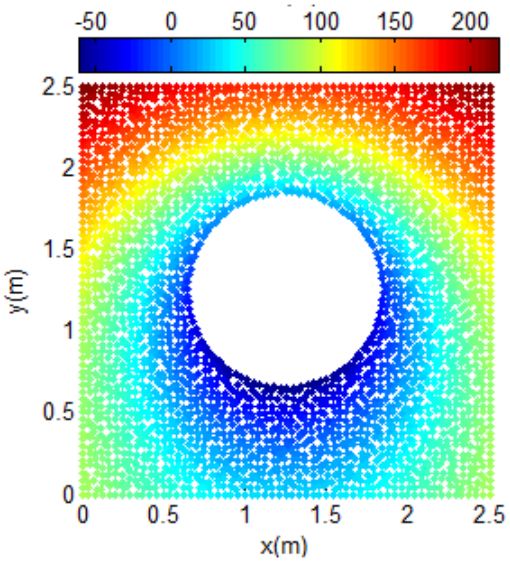

Fig. 3. Solution contours by Model 4 for the potential flow test problem.

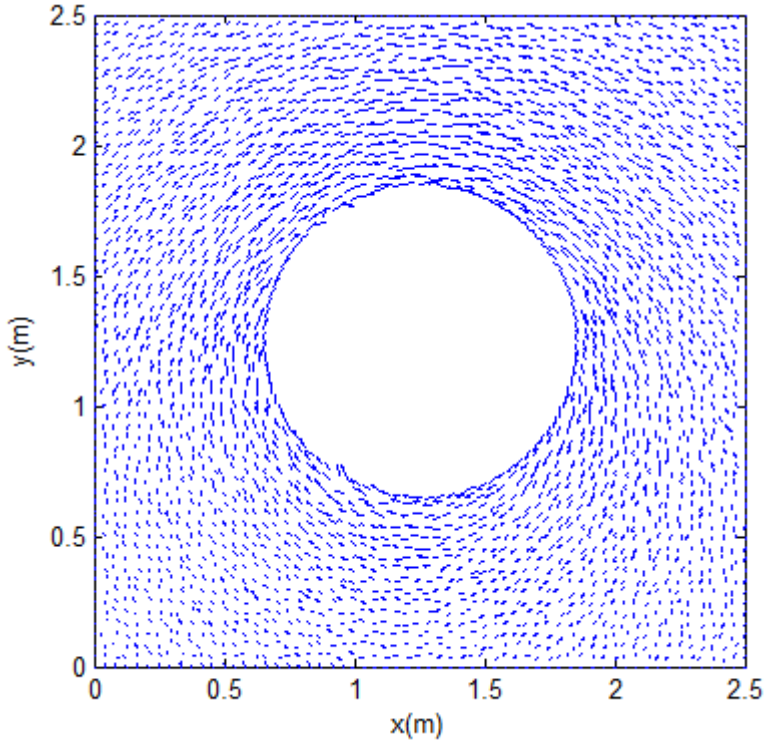

Fig. 4. Velocity field by Model 4 for the potential flow test problem.

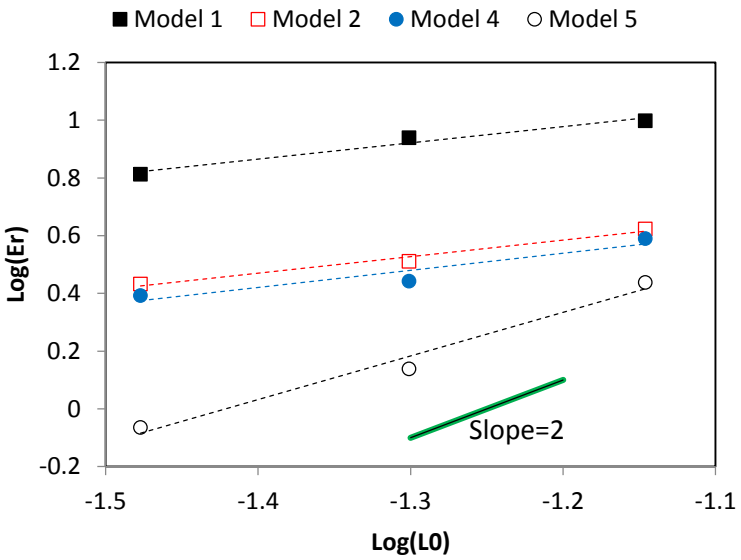

Fig. 5. Error analysis of the first PDE.

3- 2- Two-dimensional elliptic differential equations

In this section, the accuracy of the presented models is investigated for solving three 2D elliptic PDEs with different conditions. This type of differential equation describes different practical problems such as seepage flows [31]. As stated in the previous test problem, the mixed ordinary model (Model 3) is not used for the solution of the following PDEs due to its bigger errors compared with the improved mixed model (Model 4) based on the least squares scheme. The considered differential equations are given as:

$$\frac{\partial^2 f}{\partial x^2}+\frac{\partial^2 f}{\partial y^2}=2x^3-2x^2 +(y^2-y)(6x-2) \tag{30}$$

$$\frac{\partial^2 f}{\partial x^2}+\frac{\partial^2 f}{\partial y^2}=6x\sin(2\pi y) +4\pi^2\sin(2\pi y)(x-x^3) \tag{31}$$

$$\frac{\partial^2 f}{\partial x^2}+\frac{\partial^2 f}{\partial y^2}= \pi^2\sin(\pi x)(y^3-1)-6y\sin(\pi x) \tag{32}$$

The computational domain of these equations is a 1 m by 1 m square and is discretized using the method described for the potential flow test problem. The analytical solutions of Eqs. (30)-(32) are given by Eqs. (33)-(35), respectively.

$$f(x,y)=(y^2-y)(x^3-x^2) \tag{33}$$

$$f(x,y)=(x^3-x)(\sin(2\pi y)) \tag{34}$$

$$f(x,y)=(1-y^3)(\sin(\pi x)) \tag{35}$$

The first and second PDEs (Eqs. (30) and (31), respectively) have zero Dirichlet boundary conditions on all sides of the computational domain. The third PDE (Eq. (32)) has the same conditions except for the bottom side ($y=0$) where the zero Neumann boundary condition ($\partial f/\partial y=0$) is enforced in the computations. One additional node layer is required to be placed in the outer regions of the computational domain to satisfy this type of boundary condition [32] for Models 1 and 2 while Models 3, 4, and 5 can directly carry out this task.

There initial node spacing of 1/14 m, 1/20 m and 1/30 m are employed for solving the first PDE, and the corresponding errors for the models are given in Figure 5. As seen, the mixed second-order least squares model (Model 5) can achieve the highest accuracy, while the improved SPH method (Model 2) and Model 4 get almost the same accuracy which is better than that of the standard SPH method (Model 1). The results clearly show that the mixed second-order model formulated

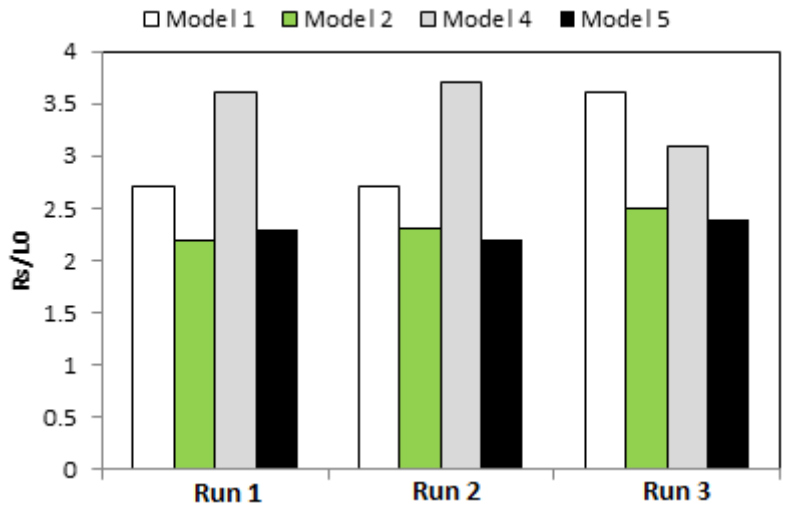

Fig. 6. Size of interaction area of the models for the solution of first PDE.

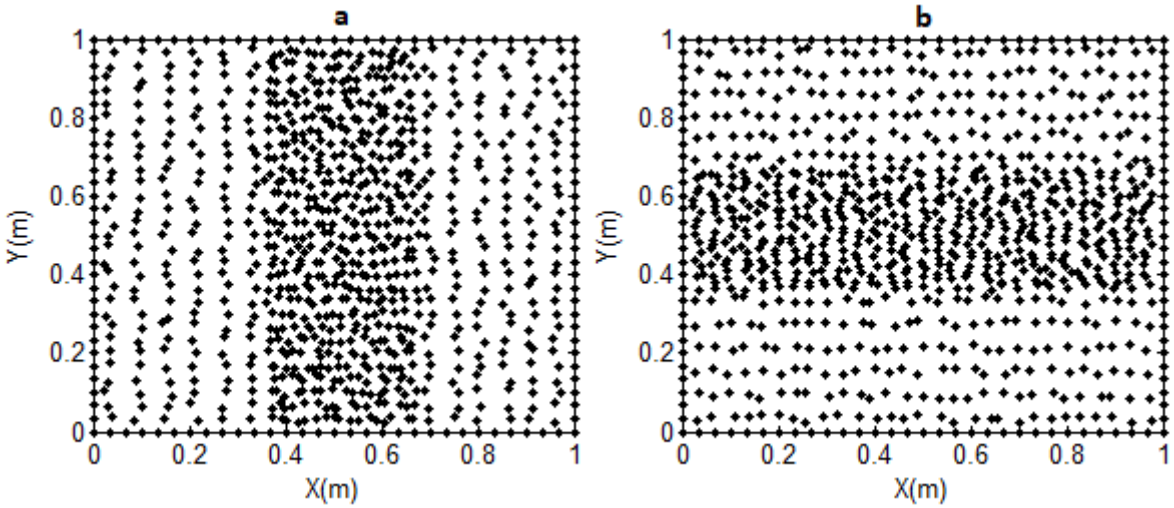

Fig. 7. The multi-resolution node distributions for the first PDE.

on the basis of the least squares concept has the ability to yield much less errors even compared with the improved SPH model which is more accurate than several well-known SPH Laplacian models [17]. In other words, it is expected that the combination of mixed and least squares schemes provides promising potential to propose different methods with significant superiority over available meshless models for the investigation of complex engineering problems.

The optimum sizes of interaction area to yield the smallest errors for the conducted runs are given for the models in Figure 6 showing better performance of Models 2 and 5. To investigate the accuracy of the models for more complex situations, two different multi-resolution node configurations shown in Figure 7 are applied for solving this PDE. The number of calculation nodes corresponds to $L_0 = 1/30$ m. Figure 8 illustrates that Model 5 can attain the most accurate results of these conditions and the corresponding solutions by this model are shown in Figure 9.

In Table 1, the CPU times and accuracy of Models 4 and 5 are compared. As seen, Model 5 can yield smaller errors with lower calculation time for $L_0 = 1/14$ m. It can be explained by the fact that Model 4 needs a larger size of interaction area ($R_s / L_0 = 3.6$) to obtain the highest accuracy. In addition to this, it can be seen that Model 4 gets the same level of accuracy of Model 5 when the finer node spacing ($L_0 = 1/20$ m) is applied leading to large calculation cost. The

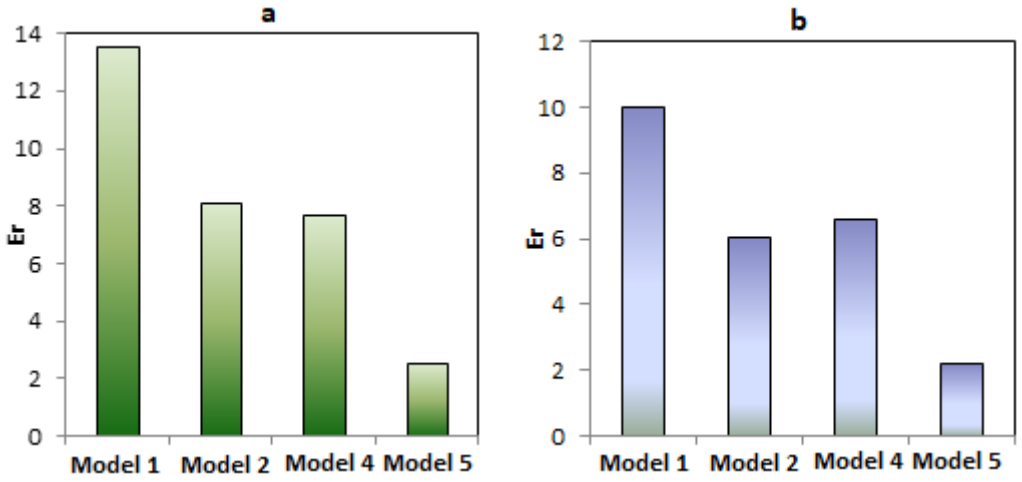

Fig. 8.Numerical errors of the models for the first PDE under node distributions of Fig. 7.

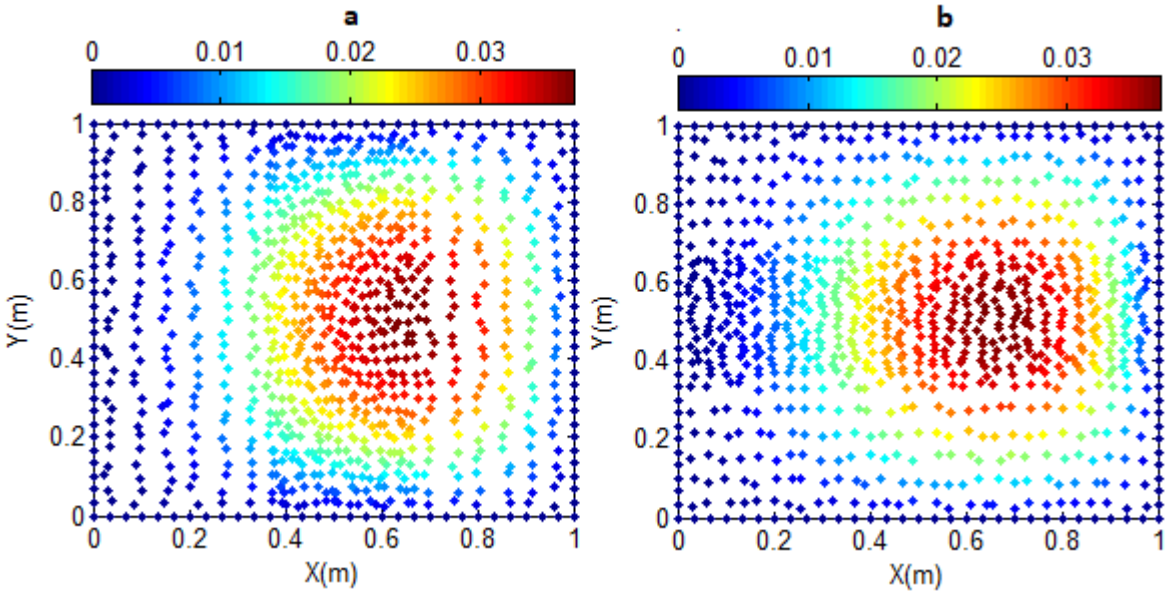

Fig. 9. Numerical solutions of the first PDE by Model 5.

Table 1. Comparison of computational efficiency of Models 4 and 5 for the first PDE.

Name of model	Model 4		Model 5
L0(m)	1/14 m	1/20 m	1/14 m
Error (%)	3.89	2.77	2.74
CPU time (s)	0.63	2.50	0.20
Size of interaction area (Rs/L0)	3.6	3.7	2.3

Table 2. Comparison of computational efficiency of Models 1, 2 and 5 for the first PDE.

Name of model	Model 1		Model 2		Model 5	
L0(m)	1/ 30 m	1/100 m	1/ 30 m	1/100 m	1/ 15 m	1/ 30 m
Error (%)	6.51	4.35	2.71	1.47	2.30	0.86
CPU time (s)	0.35	43.42	0.30	28.64	0.27	2.88
Size of interaction area (Rs/L0)	3.6	3.8	2.5	2.9	2.4	2.4

same strategy is also used to evaluate the efficiency of Models 1 and 2 exhibiting the efficiency of Model 2 as seen in Table 2. For approximately a certain CPU time (about 0.3 s), Model 5 yields higher accuracy (for $L_0 = 1/15$ m) exhibiting the superiority of this model over Model 2 using $L_0 = 1/30$ m. Model 2 with very fine node distribution ($L_0 = 1/100$ m) cannot reach the accuracy of Model 5 using $L_0 = 1/30$ m indicating again efficiency of the proposed mixed model.

Figure 10 plots the errors of the models for solving the second PDE using three average node sizes of 1/20 m, 1/30 m, and 1/40 m exhibiting again the capability of Model 5. The contour solution of the problem obtained from this model with $L_0 = 1/40$ m is depicted in Figure 11. In order to study the effect of irregularity of node distribution, values of 0.1, 0.3 and 0.5 are chosen for the irregularity index (K). Figure 12 shows that Model 2 produces a more accurate solution than Model 5 for the third PDE with $L_0 = 1/30$ m when low irregularity is used to distribute nodes (K=0.1). As seen, Model 5 get smaller errors when a larger irregularity index (K=0.3 and K=0.5) is applied exhibiting the superiority of this model over Model 2. In Figure 13, the numerical solution of the third PDE calculated by Model 5 is given. The results of Model 4 are not considered for this problem due to its lower accuracy versus Model 5. In fact, this section aims to demonstrate the effectiveness of combining the least squares scheme in the context of mixed formulation for developing an efficient meshless scheme even compared with the improved SPH method (Model 2).

4- Conclusion

This paper explores the computational superiority of the least squares scheme based on Taylor series expansion in the context of the mixed formulation over SPH method which is a meshless numerical method with many applications in the hydraulic engineering field. In this research, three enhanced models, two of which are based on the least squares scheme, in the context of mixed formulation using Taylor series expansion are presented and compared with the SPH method for the solution of different quadratic PDEs. The mixed model by converting the second-order derivative into the first-order derivative reduces the computational errors. Also using this method, one could directly calculate the first-order derivative values of the unknowns and also satisfy directly the Neumann boundary conditions. Based on the numerical performance evaluation of the models against the original and very accurate SPH Laplacian models [17], the following conclusions are drawn:

- The mixed first-order least squares model exhibits higher accuracy than the corresponding model based on mixed ordinary formulation.
- Using more terms of Taylor series expansion improves considerably efficiency of the mixed least squares model.
- The mixed first-order least squares model can achieve smaller errors even compared with the improved SPH model exhibiting significant numerical performance over several existing improved SPH schemes [17].
- The mixed second-order least squares model has substantial

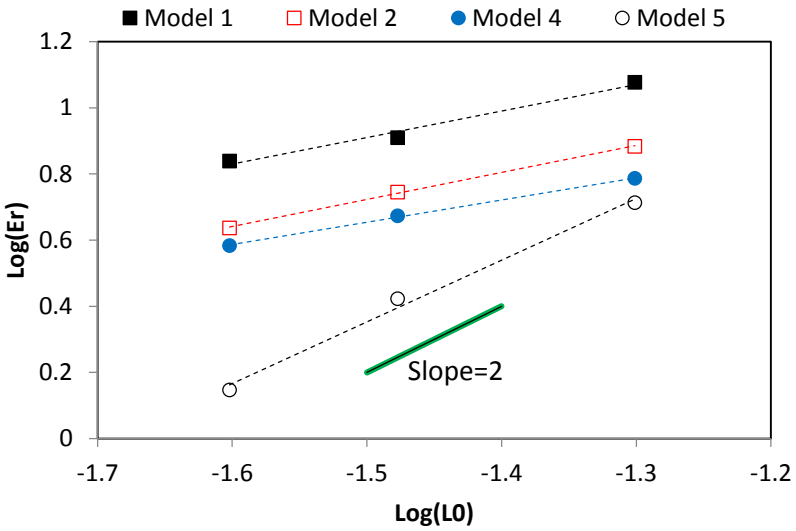

Fig. 10. Error analysis of the second PDE.

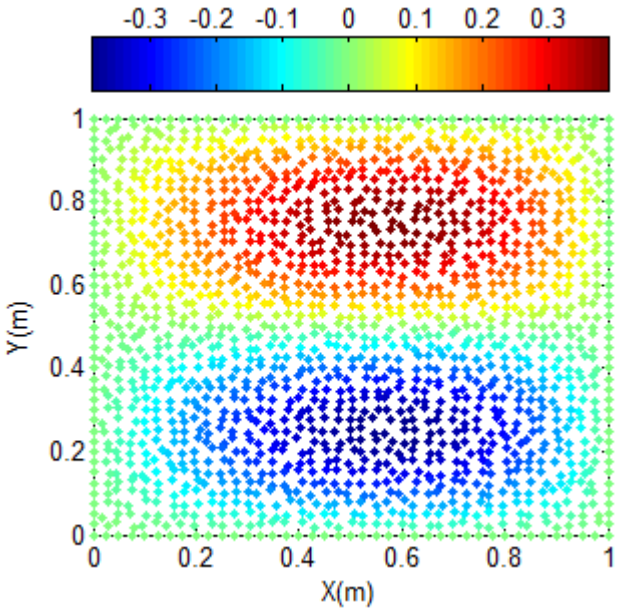

Fig. 11. Numerical solution of the second PDE by Model 5.

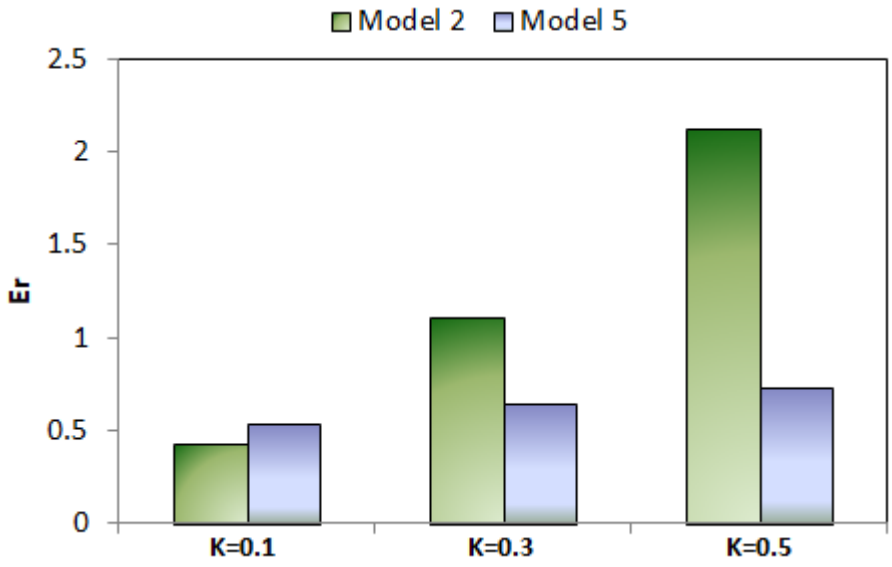

Fig. 12. Error analysis of the third PDE for different irregularity index.

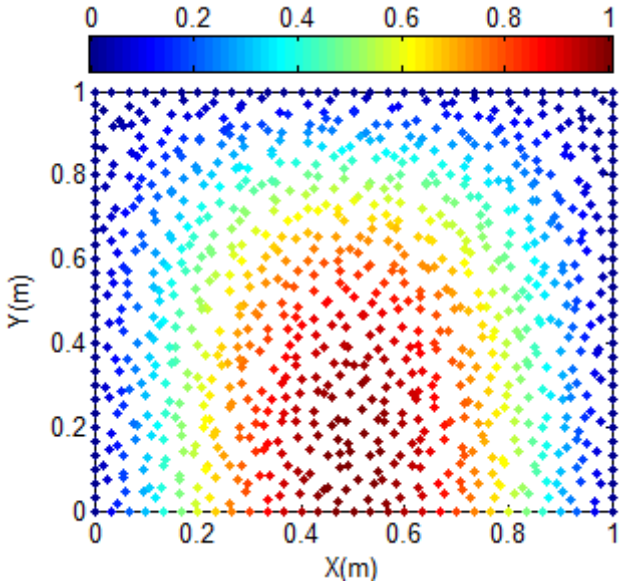

Fig. 13. Numerical solution of the third PDE calculated by Model 5.

computational efficiency over the improved SPH scheme. In other words, this model needs a lower number of computational nodes and thus reduces the computational cost with better precision.

References

[1] R.A. Gingold, J.J. Monaghan, Smoothed particle hydrodynamics: theory and application to non-spherical stars, Monthly notices of the royal astronomical society, 181(3) (1977) 375-389.

[2] J.J. Monaghan, Simulating free surface flows with SPH, Journal of computational physics, 110(2) (1994) 399-406.

[3] S. Shao, E.Y. Lo, Incompressible SPH method for simulating Newtonian and non-Newtonian flows with a free surface, Advances in water resources, 26(7) (2003) 787-800.

[4] E. Kazemi, K. Koll, S. Tait, S. Shao, SPH modelling of turbulent open channel flow over and within natural gravel beds with rough interfacial boundaries, Advances in Water Resources, 140 (2020) 103557.

[5] Z. Heydari, G. Shobeyri, S. H. G. Najafabadi, Numerical investigation of solitary wave interaction with a flapper wave energy converter using incompressible SPH method, Journal of the Brazilian Society of Mechanical Sciences and Engineering, 43 (2021)1-18.

[6] Y. Pan, X. Yang, S. C. Kong, F. C. Ting, C. Iyer, J. Yi, Characterization of fuel drop impact on wall films using SPH simulation. International Journal of Engine Research, 23(3) (2022) 416-433.

[7] Y. Shimizu, A. Khayyer, H. Gotoh, An enhanced incompressible SPH method for simulation of fluid flow interactions with saturated/unsaturated porous media of variable porosity, Ocean Systems Engineering, 12(1) (2022) 63-86.

[8] X. Dong, G. Hao, R. Yu, Two-dimensional smoothed particle hydrodynamics (SPH) simulation of multiphase melting flows and associated interface behavior, Engineering Applications of Computational Fluid Mechanics, 16(1) (2022) 588-629.

[9] Z. Tan, P.N. Sun, N.N. Liu, Z. Li, H.G. Lyu, R.H. Zhu, SPH simulation and experimental validation of the dynamic response of floating offshore wind turbines in waves, Renewable Energy, 205 (2023) 393-409.

[10] X. Zheng, M. Rubinato, X. Liu, Y. Ding, R. Chen, E. Kazemi, SPH Simulation of Sediment Movement from Dam Breaks, Water, 15(17) (2023) 3033.

[11] Z. Heydari, G.Shobeyri, S. H. G. Najafabadi, Accuracy analysis of different higher-order Laplacian models of Incompressible SPH method. Engineering Computations, 37(1) (2020) 181-202.

[12] X. Hu, N.A. Adams, An incompressible multi-phase SPH method, Journal of computational physics, 227(1) (2007) 264-278.

[13] H.F. Schwaiger, An implicit corrected SPH formulation for thermal diffusion with linear free surface boundary conditions, International Journal for Numerical Methods in Engineering, 75(6) (2008) 647-671.

[14] S.M. Hosseini, J.J. Feng, Pressure boundary conditions for computing incompressible flows with SPH, Journal of Computational physics, 230(19) (2011) 7473-7487.

[15] G. Shobeyri, Improving accuracy of Laplacian model of incompressible SPH method using higher-order interpolation, Iranian Journal of Science and Technology, Transactions of Civil Engineering, 43(4) (2019) 791-805.

[16] G. Shobeyri, Accuracy analysis of different Laplacian models of incompressible SPH method improved by using Voronoi diagram, Journal of the Brazilian Society of Mechanical Sciences and Engineering, 42(10) (2020) 1-14.

[17] G. Shobeyri, Using a modified MPS gradient model to improve accuracy of SPH method for Poisson equations, Computational Particle Mechanics, 5 (2023) 1113-1126.

[18] G. R. Liu , Meshfree methods: moving beyond the finite element method. CRC press, 2009.

[19] S. Faraji, M.H. Afshar, J. Amani, Mixed discrete least square meshless method for solution of quadratic partial differential equations, Scientia Iranica, 21 (2014) 492–504.

[20] S. Faraji, M. Kolahdoozan, M.H. Afshar, Mixed Discrete Least Squares Meshless method for solving the linear and non-linear propagation problems, Scientia Iranica, 25(2) (2018) 565-578.

[21] S. Faraji, M. Kolahdoozan, M.H. Afshar, Collocated mixed discrete least squares meshless (CMDLSM) method for solving quadratic partial differential equations, Scientia Iranica 25(4) (2018) 2000-2011.

[22] S. Faraji, M. Kolahdoozan, M. Afshar, Mixed Discrete Least Squares Meshfree method for solving the incompressible Navier–Stokes equations, Engineering analysis with boundary elements, 88 (2018) 64-79.

[23] S. Faraji, M. Kolahdoozan, M.H. Afshar, S. Dabiri, An Eulerian–Lagrangian mixed discrete least squares meshfree method for incompressible multiphase flow problems, Applied Mathematical Modelling, 76 (2019) 193–224.

[24] N. Eini, M. Afshar, S. Faraji, G. Shobeyri, A. Afshar, A fully Lagrangian mixed discrete least squares meshfree method for simulating the free surface flow problems, Engineering with Computers, (2020) 1-21.

[25] H. Arzani, M. Afshar, Solving Poisson's equations by the discrete least square meshless method, WIT Transactions on Modelling and Simulation, 42 (2006) 23-31.

[26] X. Zheng, W. Y. Duan, Q. W. Ma, Comparison of improved meshless interpolation schemes for SPH method and accuracy analysis, Journal of Marine Science and Application, 9(3) (2010) 223-230.

[27] X. Zheng, Q. Ma, S. Shao, A. Khayyer, Modelling of violent water wave propagation and impact by

incompressible SPH with first-order consistent kernel interpolation scheme. Water, 9(6) (2017) 400.

[28] G. Shobeyri, Mixed smoothed particle hydrodynamics method for planar elasticity problems. Iranian Journal of Science and Technology, Transactions of Civil Engineering, 47(1) (2023) 491-504.

[29] C. G. Koh, M. Gao, C. Luo, A new particle method for simulation of incompressible free surface flow problems. International journal for numerical methods in engineering, 89(12) (2012) 1582-1604.

[30] K. Roushangar, S. Shahnazi, A. A. Sadaghiani, An efficient hybrid grey wolf optimization-based KELM approach for prediction of the discharge coefficient of submerged radial gates, Soft Computing, 27(7) (2023) 3623-3640.

[31] R. Daneshfaraz, S. Sadeghfam, R. Adami, H. Abbaszadeh, Numerical Analysis of Seepage in Steady and Transient Flow State by the Radial Basis Function Method, Numerical Methods in Civil Engineering, 8(1) (2023) 58-68.

[32] S. Koshizuka, A. Nobe, Y. Oka, Numerical analysis of breaking waves using the moving particle semi-implicit method, International journal for numerical methods in fluids 26(1998) 751–69.

HOW TO CITE THIS ARTICLE

Gh. R. Shobeyri, S. H. Ghoreishi Najafabadi, M. Abed, Computational efficiency of mixed least squares meshless models over SPH method for elliptic PDEs , AUT J. Civil Eng., 8(1) (2024) 17-32.

DOI: 10.22060/ajce.2024.22777.5847